

## PATTERN SOLUTIONS OF THE KLAUSMEIER MODEL FOR BANDED VEGETATION IN SEMIARID ENVIRONMENTS IV: SLOWLY MOVING PATTERNS AND THEIR STABILITY\*

JONATHAN A. SHERRATT†

**Abstract.** Banded vegetation is a characteristic feature of semiarid environments, comprising stripes of vegetation running parallel to the contours on hillsides, separated by stripes of bare ground. Mathematical modelling plays an important role in the study of this phenomenon, and the Klausmeier model is one of the oldest and most established, consisting of coupled reaction-diffusion-advection equations for plant biomass and water density. In this model the dimensionless parameter corresponding to slope gradient is much larger than the other parameters, and this paper is part of a series investigating the asymptotic form of pattern solutions for large values of the slope parameter. The pattern solutions move uphill with a constant speed,  $c$  say, and the focus of this paper is  $c = O(1)$ . I begin by deriving the leading order form of the patterns, and the region of parameter space in which they occur, for  $c = o(1)$ . Using this, I show that all patterns with  $c = o(1)$  are unstable as model solutions for sufficiently large values of the slope parameter. I then consider patterns with  $c = O_s(1)$ , showing that this region of parameter space contains both stable and unstable low amplitude patterns. I conclude by discussing the ecological implications of my results.

**Key words.** pattern formation, reaction diffusion advection, stability, perturbation theory, arid landscapes, Lamé’s equation, Weierstrass elliptic function

**AMS subject classifications.** 92D40, 35C07, 35M10

**DOI.** 10.1137/120862648

**1. Introduction.** Banded vegetation is a characteristic feature of semiarid environments [1, 2]. In this phenomenon, stripes of vegetation occur on hillsides, running parallel to the contours, separated by stripes of bare ground. Banded vegetation is hard to detect on the ground, and was first recognized during flights over sub-Saharan Africa in the 1950s [3]. It is now known to occur in many parts of the world, particularly Australia [4], Mexico/southwestern U.S. [5], and Africa [3, 6]. Typical wavelengths are about 1km for trees and shrubs, with shorter wavelengths for grasses.

Mathematical modelling plays a key role in the study of banded vegetation, because field studies are difficult and there are no equivalent laboratory systems. This paper concerns one of the oldest and most established models, due to Klausmeier [7]:

$$\begin{aligned}
 (1.1a) \quad \partial u / \partial t &= \overbrace{wu^2}^{\text{plant growth}} - \overbrace{Bu}^{\text{plant loss}} + \overbrace{\partial^2 u / \partial x^2}^{\text{plant dispersal}}, \\
 (1.1b) \quad \partial w / \partial t &= \underbrace{A}_{\text{rain-fall}} - \underbrace{w}_{\text{evap-oration}} - \underbrace{wu^2}_{\text{uptake by plants}} + \underbrace{\nu \partial w / \partial x}_{\text{flow downhill}}.
 \end{aligned}$$

In this dimensionless formulation,  $u(x, t)$  is plant density,  $w(x, t)$  is water density,  $t$  is time, and  $x$  is a one-dimensional space variable running in the uphill direction. The

---

\*Received by the editors January 17, 2012; accepted for publication (in revised form) October 10, 2012; published electronically February 5, 2013. This work was supported in part by a Leverhulme Trust Research Fellowship.

<http://www.siam.org/journals/siap/73-1/86264.html>

†Department of Mathematics and Maxwell Institute for Mathematical Sciences, Heriot-Watt University, Edinburgh EH14 4AS, UK (jas@ma.hw.ac.uk).

parameters  $A$ ,  $B$ , and  $\nu$  can be most usefully interpreted as reflecting rainfall, plant loss, and slope gradient, respectively, although of course they represent a combination of ecological quantities (see [7, 8] for details). The basic hypothesis underlying the Klausmeier model (1.1) is that banded vegetation forms as a result of water redistribution, and there are a number of subsequent models based on the same hypothesis. Most of these represent soil and surface water separately [9, 10, 11], and some incorporate features such as herbivory or rainfall variability [12, 13]. There is also another class of models, which assume that the cause of banded vegetation is a short range activation and long range inhibition process, arising from the different length scales of tree/shrub crowns and their root systems [14].

These various modelling studies are almost entirely simulation based. Other than my own work [15, 16, 17], the only paper that I am aware of containing nonlinear analysis of a banded vegetation model is [18], which proves an existence theorem for the model of Gilad et al. [10]. In particular, for the Klausmeier model (1.1) there are no analytical results beyond linear stability of spatially homogeneous solutions [7, 8]. This paper is the fourth in a series attempting to develop a detailed analytical understanding of pattern solutions of (1.1). Such a study is possible because typical values of the slope parameter  $\nu$  (about 200 [7]) are significantly larger than the rainfall parameter  $A$  (0.1–3.0 [7, 9]) and the plant loss parameter  $B$  (0.05–2.0 [7, 9]). This permits patterned solutions of (1.1) to be studied using perturbation theory. My approach assumes formal expansions for the pattern solutions; an alternative would be to use geometric singular perturbation theory [19], which has proved successful in studying patterns in other reaction-diffusion systems [20, 21]. Note that the large value of the dimensionless parameter  $\nu$  reflects the advection rate of water being much larger than the plant dispersal rate. In particular, the slope itself is not steep, and, indeed, on gradients above a few percent, rainwater generates gullies and (1.1) does not apply.

Numerical simulations show that pattern solutions of (1.1) move in the positive  $x$  direction (uphill) at a constant speed. This migration has been the subject of a long ecological debate (see [22, pp. 24–26] for a detailed discussion). A considerable number of field studies do report uphill migration [1, Table 5], [23], with the proposed cause being higher moisture levels on the uphill edge of the bands than on their downhill edge, leading to reduced plant death and greater seedling density [22, 24]. However, there is also contradictory data reporting stationary patterns [4, 6, 25]. A possible resolution of this discrepancy could be that in these latter cases, the relevant migration speeds are simply very low and thus went undetected. A key conclusion of this paper will be that this explanation is inconsistent with the model (1.1).

The constant uphill migration of the patterns means that an appropriate solution ansatz for (1.1) is  $u(x, t) = U(z)$ ,  $w(x, t) = W(z)$ , with  $z = x - ct$ , which gives

$$(1.2a) \quad d^2U/dz^2 + c dU/dz + WU^2 - BU = 0,$$

$$(1.2b) \quad (\nu + c)dW/dz + A - W - WU^2 = 0.$$

Patterns correspond to periodic (limit cycle) solutions of (1.2), and their mathematical properties depend fundamentally on the way in which the migration speed  $c > 0$  scales with the (large) slope parameter  $\nu$ . In previous papers, I have considered the case of large  $c$ , specifically  $c = O_s(\nu)$  [16],  $\nu \gg c \gg \nu^{1/2}$  [15], and  $c = O_s(\nu^{1/2})$  [17], as  $\nu \rightarrow \infty$ . Note that the notation  $f = O_s(g)$  denotes  $f = O(g)$  and  $f \neq o(g)$ . In this paper, I study the case  $c = O(1)$ . In section 2, I describe numerical results on the parameter region giving patterns. In sections 3, 4, and 5, I present analysis of the existence and form of patterns for  $c = O_s(1/\nu)$ ,  $c = o(1/\nu)$ , and  $1/\nu \ll c \ll 1$ ,

respectively. In section 6, I use these results on pattern form as the basis for an investigation of pattern stability, showing that all patterns with  $c \ll 1$  as  $\nu \rightarrow \infty$  are unstable as solutions of (1.1). In section 7, I consider  $c = O_s(1)$ , proving that this parameter region contains both stable and unstable patterns. These various results are valid to leading order for large values of the slope parameter  $\nu$ . In section 8, I discuss the ecological implications of my results.

**2. The parameter region giving patterns.** Numerical simulations of (1.1) suggest that, for given values of  $B$  and  $\nu$ , there is a range of values of the rainfall parameter  $A$  giving patterns [7, 8, 26]. Intuitively, sufficiently high rainfall levels give homogeneous vegetation, while sufficiently low levels give full-blown desert; between these extremes there are banded vegetation patterns.

Straightforward calculation shows that in addition to the “desert” steady state  $(0, A)$ , (1.1) has two homogeneous vegetated equilibria when  $A \geq 2B$ :

$$(2.1) \quad (u_{\pm}, w_{\pm}) = \left( \frac{A \pm \sqrt{A^2 - 4B^2}}{2B}, \frac{A \mp \sqrt{A^2 - 4B^2}}{2} \right).$$

Numerical bifurcation studies [16, 27] suggest that the upper end of the rainfall range giving patterns corresponds to a supercritical Hopf bifurcation of one of  $(u_{\pm}, w_{\pm})$  in (1.2). The solution branch terminates at a homoclinic solution, so that the lower end of the rainfall range giving patterns corresponds either to this homoclinic solution, or to a fold in the solution branch. Figure 2.1(a) illustrates the region of the  $A$ - $c$

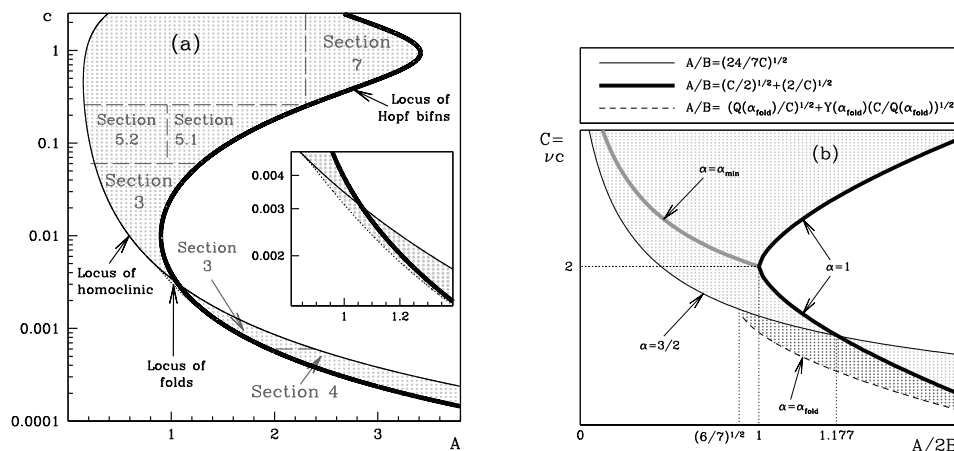


FIG. 2.1. (a) The region of the  $A$ - $c$  parameter plane in which (1.1) has patterned solutions (indicated by light gray dots). Note the logarithmic scale on the  $c$ -axis. The thick curve is the locus of Hopf bifurcations in (1.2). The thin solid curve is the locus of homoclinic solutions of (1.2). The dotted curve is the locus of folds in the branch of periodic solutions of (1.2); this is shown more clearly in the inset, which is a magnification of the part of the parameter plane containing the fold locus. These various curves were calculated by numerical continuation, using AUTO [28]. The dark gray dashed lines indicate the approximate division of the pattern region into subregions considered in different parts of the paper. Note that the subregion in the upper left-hand corner of the figure is not considered in this paper and will be discussed in a subsequent publication. Note also that the parameter region giving patterns does extend significantly above the part shown in this figure, up to  $c \approx 54$ ; details of patterns for large speeds are given in [15, 16]. The other parameter values are  $B = 0.45$  and  $\nu = 200$ . (b) A schematic illustration of the curves determining the parameter region giving one (light gray dots) or two (dark gray dots) pattern solutions when  $c = O_s(1/\nu)$  as  $\nu \rightarrow \infty$ .

parameter plane giving patterns for the low and moderate wave speeds considered in this paper.

The first step in investigating patterns for large  $\nu$  is to calculate the leading order form of the Hopf bifurcation locus. To do this, I calculated the (cubic) eigenvalue equation at  $(u_{\pm}, w_{\pm})$  and imposed the requirement of a complex conjugate pair of roots with zero real part. For  $c = O(1)$  as  $\nu \rightarrow \infty$ , this gives

$$(2.2a) \quad c = o(1/\nu) : \quad A = O_s(c^{-1/2}\nu^{-1/2}), \quad c = 2B^2/(A^2\nu),$$

$$(2.2b) \quad c = O_s(1/\nu) : \quad A = O_s(1), \quad c = \left(A - \sqrt{A^2 - 4B^2}\right)^2 / (2B^2\nu) \quad (A \geq 2B),$$

$$(2.2c) \quad \text{and} \quad c = \left(A + \sqrt{A^2 - 4B^2}\right)^2 / (2B^2\nu) \quad (A \geq 2B),$$

$$(2.2d) \quad 1/\nu \ll c \ll 1 : \quad A = O_s(\nu^{1/2}c^{1/2}), \quad c = 2A^2/(B^2\nu),$$

$$(2.2e) \quad c = O_s(1) : \quad A = O_s(\nu^{1/2}), \quad c = \frac{A^2}{2B^2\nu} + \frac{B^3\nu}{2A^2} \pm \left[ \frac{A^4}{4B^4\nu^2} + \frac{B^6\nu^2}{4A^4} - \frac{3B}{2} \right]^{1/2} \\ (A < [\sqrt{2} - 1]^{1/2}B^{5/4}\nu^{1/2}).$$

Here the Hopf bifurcation is of  $(u_-, w_-)$  for (2.2a), (2.2b), and of  $(u_+, w_+)$  for (2.2c)–(2.2e). Note that there is consistency between (2.2a) and (2.2b), and between (2.2c) and (2.2d), because  $(A \pm \sqrt{A^2 - 4B^2})^2 / (2B^2) \sim 2(A/B)^{\pm 2}$  as  $A \rightarrow \infty$ .

**3. Pattern solutions for  $c = O_s(1/\nu)$ .** In this section, I will show formally that for  $c = O_s(1/\nu)$ , patterns exist only if  $A = O_s(1)$ , with the leading order conditions for patterns being as illustrated schematically in Figure 2.1(b). Note that for some parameter values there are two different pattern solutions. I write

$$(3.1a) \quad U(z) = U_0(z) + \nu^{-1}U_1(z) + \nu^{-2}U_2(z) + \text{h.o.t.},$$

$$(3.1b) \quad W(z) = W_0(z) + \nu^{-1}W_1(z) + \nu^{-2}W_2(z) + \text{h.o.t.},$$

$$(3.1c) \quad L = L_0 + \nu^{-1}L_1 + \nu^{-2}L_2 + \text{h.o.t.},$$

where  $L$  is the pattern wavelength. Here and throughout the paper, I use h.o.t. to denote “higher order terms.” I also impose

$$(3.2) \quad U'(0) = 0 \quad \text{and} \quad U''(0) < 0,$$

which specify the solution uniquely, since I will show that all patterns have only one local maximum and minimum for  $U$  per period. Substituting (3.1a), (3.1b) into (1.2) gives the leading order equations  $W'_0 = 0 \Rightarrow W_0 = k_0$ , say, and

$$(3.3) \quad U''_0 + k_0U_0^2 - BU_0 = 0 \quad \Rightarrow U_0 = (B/k_0)U^*(B^{1/2}z; \alpha),$$

$$(3.4) \quad \text{where } (dU^*(\xi; \alpha)/d\xi)^2 + \frac{2}{3}U^{*3} - U^{*2} = \frac{2}{3}\alpha^3 - \alpha^2.$$

Here  $k_0 > 0$  and  $\alpha$  are constants of integration. In the following, I will often omit the specification of the  $\alpha$ -dependence in  $U^*$ , for brevity. Note that rescaling  $z$  and  $W$  by  $B^{1/2}$  and  $B^{-1}$ , respectively, in (1.2a) is natural if  $W$  is constant, since it enables the elimination of one parameter. Equation (3.4) has a unique nonconstant solution satisfying (3.2), which is linearly related to the Weierstrass elliptic function

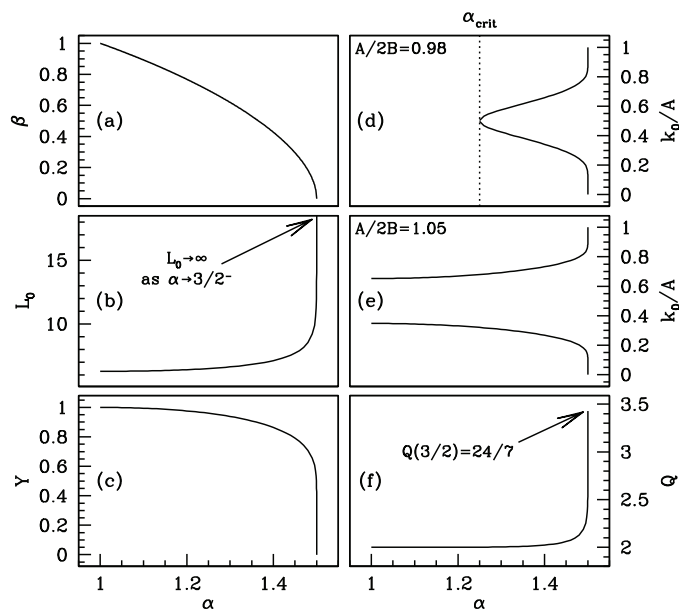


FIG. 3.1. Plots of the variation with  $\alpha$  of  $\beta$ ,  $L_0$ ,  $Y$ ,  $k_0$ , and  $Q$ . The constant  $k_0$  depends on  $A$  and  $B$  as well as on  $\alpha$ , and there are two qualitatively different cases, for  $A/2B < 1$  and  $A/2B > 1$ ; I show a representative example of each case. To evaluate the integrals in (3.6) and (A.8), I used the software package MAPLE. For accurate computations, a large number of decimal places is required: I used `digits = 40`, with error tolerance `epsilon = 10-20`. An alternative method of calculating  $Y$  is discussed in Appendix A.3.

(see section 6.1 for details). The solution has a local maximum  $U^* = \alpha$  at  $z = 0$  and a local minimum at  $U^* = \beta = \frac{1}{4}[3 - 2\alpha + \{9 + 12\alpha - 12\alpha^2\}^{1/2}]$  ( $0 < \beta < 1$ ). In Appendix A.3, I show that the period  $L_0$  of  $U_0$  is an increasing function of  $\alpha$ . Figures 3.1(a) and 3.1(b) illustrate the dependence of  $\beta$  and  $L_0$  on  $\alpha$ . As  $\alpha \rightarrow 1^+$ ,  $\beta \rightarrow 1$  also, so that the solution is constant in this limit, which corresponds to a Hopf bifurcation in the travelling wave equations (1.2). As  $\alpha \rightarrow \frac{3}{2}^-$ ,  $L_0 \rightarrow \infty$  so that this is a homoclinic limit. My basic approach to studying pattern solutions in this parameter regime is to use  $\alpha$  to parameterize the solution branches between these two end points.

The calculation of the leading order pattern solution has been straightforward, but the constants of integration  $k_0$  and  $\alpha$  are undetermined. The solutions for  $U_1$  and  $W_1$  are required in order to specify these constants. Substituting (3.1a), (3.1b) into (1.2b) and equating terms that are  $O_s(1)$  as  $\nu \rightarrow 0$  gives

$$(3.5) \quad dW_1/dz + A - k_0 - k_0 U_0^2 = 0.$$

Periodicity of  $W_1$  requires that  $[W_0(z) + \nu^{-1}W_1(z)]_{z=-(L_0+\nu^{-1}L_1)/2}^{z=(L_0+\nu^{-1}L_1)/2} = O(\nu^{-2}) \Rightarrow W_1(-L_0/2) = W_1(L_0/2)$ . Integrating (3.5) between  $-L_0/2$  and  $L_0/2$  therefore implies

$$(3.6) \quad k_0(A - k_0)/B^2 = Y(\alpha) \equiv 1 / \left( L_0 B^{1/2} \right) \int_{\xi=-L_0 B^{1/2}/2}^{\xi=L_0 B^{1/2}/2} U^*(\xi)^2 d\xi;$$

note that  $L_0 B^{1/2}$  is a function of  $\alpha$  only, independent of other parameters. In Appendix A.3, I prove that  $Y(\alpha)$  is increasing; Figure 3.1(c) illustrates its form. Equation

(3.6) determines  $k_0$  as a function of  $\alpha$  (illustrated in Figures 3.1(d) and 3.1(e)). If  $A > 2B$ , there are two possible values of  $k_0$  for each  $\alpha \in (1, 3/2)$ . In the limit  $\alpha \rightarrow 1^+$ , the two solutions lie on either side of  $A/2$ ; from (2.1) it follows that the larger/smaller values of  $k_0$  correspond to a solution branch resulting from a Hopf bifurcation of  $(u_-, w_-)/(u_+, w_+)$ . For  $A < 2B$  there are two solutions for  $\alpha > \alpha_{min}$  and none for  $\alpha < \alpha_{min}$ , where  $\alpha_{min}$  is defined by  $Y(\alpha_{min}) = A^2/4B^2$ . For these values of  $A/2B$  there is no Hopf bifurcation, and indeed the steady states  $(u_{\pm}, w_{\pm})$  do not exist.

It remains to calculate the dependence of the wave speed on  $\alpha$ , and this comes from consideration of  $U_1$ . I write  $C = \nu c$  so that  $C = O_s(1)$  as  $\nu \rightarrow \infty$ . Then substituting (3.1a) and (3.1b) into (1.2a) and equating terms that are  $O_s(\nu^{-1})$  gives

$$(3.7) \quad U_1'' + CU_1' + 2k_0U_0U_1 + W_1U_0^2 - BU_1 = 0.$$

By manipulating (3.7) and integrating over a whole period, the unknown solution  $U_1$  can be eliminated to give a formula for  $C$  (see Appendix A.1 for details):

$$(3.8) \quad C = \left(\frac{B}{k_0}\right)^2 Q(\alpha), \quad \text{where } Q(\alpha) = \frac{2}{7} \left[ 2 - 7Y(\alpha) + \frac{10(2\alpha^3 - 3\alpha^2 + 1)Y(\alpha)}{2\alpha^3 - 3\alpha^2 + Y(\alpha)} \right].$$

Figure 3.1(f) illustrates the dependence of  $Q$  on  $\alpha$ .

This completes the calculation of the leading order form of patterns as  $\nu \rightarrow \infty$  with  $c = O_s(1/\nu)$ . However, interpretation of these solutions is not straightforward. I will use them to determine the region of the  $A$ - $c$  parameter plane in which patterns exist (illustrated schematically in Figure 2.1(b)). First I consider the case of  $A$  fixed and  $> 2B$  and determine how  $C$  varies along each of the two branches of pattern solutions, from the Hopf bifurcation ( $\alpha = 1$ ) to the homoclinic solution ( $\alpha = 3/2$ ); recall that the two branches correspond to the two roots of (3.6) for  $k_0$ . The smaller root for  $k_0$  has  $dk_0/d\alpha < 0$  with  $k_0 \rightarrow 0$  as  $\alpha \rightarrow \frac{3}{2}^-$ , and a combination of analysis and numerical calculations in Appendices A.2 and A.3 indicates that  $Q$  is an increasing function of  $\alpha$ ; also  $Q(3/2)$  is finite. Therefore  $C$  increases along this solution branch, from the Hopf bifurcation value given in (2.2c) to infinity.

For the larger root for  $k_0$ , the variation in  $C$  with  $\alpha$  is not monotonic. I define  $C_{\text{hopf}} \equiv C|_{\lim \alpha \rightarrow 1^+}$  and  $C_{\text{hc}} \equiv C|_{\lim \alpha \rightarrow 3/2^-}$  along this solution branch. In Appendix A.2, I show that  $C_{\text{hc}} < C_{\text{hopf}} \Leftrightarrow (A/2B) < [3/(2\sqrt{21} - 7)] = 1.177\dots$ , and that as  $\alpha \rightarrow 3/2^-$ ,  $C(\alpha)$  approaches  $C_{\text{hc}}$  from below  $\Leftrightarrow (A/2B) > \sqrt{6/7} = 0.9258\dots$ . Therefore, for  $A/2B \in (0.9258, 1.177)$ ,  $C$  has a local minimum  $C_{\text{fold}}$  at  $\alpha = \alpha_{\text{fold}} \in (1, 3/2)$ . Numerical calculations indicate that this local minimum is unique, and numerical continuation of it shows that it terminates at  $A/2B = 0.9258$  (when  $\alpha_{\text{fold}} = 1$ ). The conclusion from this combination of analysis and numerical results is that along this solution branch,  $C$  initially decreases from the Hopf bifurcation value given in (2.2b) ( $\alpha = 1$ ) up to a fold at  $C = C_{\text{fold}}$ ,  $\alpha = \alpha_{\text{fold}}$ . Beyond this  $C$  increases to  $C_{\text{hc}}$ , which will be above or below the starting value  $C_{\text{hopf}}$  for  $A/2B > 1.177$  and  $A/2B < 1.177$ , respectively.

For  $A < 2B$  there cannot be a Hopf bifurcation in the travelling wave equation as  $c$  is varied, since the steady states  $(u_{\pm}, w_{\pm})$  do not exist. As  $\alpha$  is increased from  $\alpha_{min}$ , the value of  $C$  corresponding to the smaller solution for  $k_0$  increases without bound. For the larger solution for  $k_0$ ,  $C$  initially decreases as  $\alpha$  increases above  $\alpha_{min}$ . If  $A/2B < \sqrt{6/7}$ , this decrease is monotonic to  $C_{\text{hc}}$ , while for  $A/2B \in (\sqrt{6/7}, 1)$  there is a fold at  $\alpha = \alpha_{\text{fold}}$ ,  $C = C_{\text{fold}}$ , beyond which  $C$  increases up to  $C_{\text{hc}}$  ( $< C_{\text{hopf}}$ ).

Note that an important difference between the  $A > 2B$  and  $A < 2B$  cases is that for  $A > 2B$  the two solution branches start ( $\alpha = 1$ ) at different values of  $C$ , with no pattern solutions for values of  $C$  between the starting points. For  $A < 2B$  the starting points ( $\alpha = \alpha_{min}$ ) have a common value of  $C$ .

**4. Pattern solutions for  $c = o(1/\nu)$ .** The scaling  $c = o(1/\nu)$  gives patterns with the smallest wave speeds. I will show formally that to leading order for large  $\nu$ , patterns exist in a strip bounded by the Hopf bifurcation locus  $c = B^2Q(1)/(\nu A^2) = 2B^2/(\nu A^2)$  and the homoclinic locus  $c = B^2Q(3/2)/(\nu A^2) = 24B^2/(7\nu A^2)$ . Derivation of this is very similar to the work presented in section 3, and I present only a brief outline; details are available in [31]. The leading order solution for large  $\nu$  is  $U = (B/A)U^*(B^{1/2}z; \tilde{\alpha})$ ,  $W = A$ . Here  $\tilde{\alpha} \in (1, \frac{3}{2})$  parameterizes the solution branch. The wave speed  $c$  is determined by higher order terms, and both  $O(c)$  and  $O(\nu c)$  corrections must be considered; these imply  $c = (B^2/A\nu)Q(\tilde{\alpha})$ , to leading order for large  $\nu$ . A combination of analysis and computation indicates that  $Q$  is an increasing function of  $\alpha$  (see Appendix A.3), and the conditions for pattern existence then follow.

**5. Pattern solutions for  $1/\nu \ll c \ll 1$ .** In this section, I will show formally that to leading order for large  $\nu$ , the condition for pattern existence is  $24B^2/7\nu c < A^2 < \frac{1}{2}B^2\nu c$ . Three different cases must be considered, according to the way in which the rainfall  $A$  scales with  $\nu$ .

**5.1. The case  $A^2 = O_s(\nu c)$ .** This parameter region again has strong similarities to the region considered in section 3, and I omit details of the calculations, which are given in [31]. The leading order solution is  $W_0$  constant and  $U_0 = AU^*(B^{1/2}z; \hat{\alpha})/(BY(\hat{\alpha}))$  ( $\hat{\alpha} \in (1, \frac{3}{2})$ ), with  $c = A^2B^{-2}\nu^{-1}Q(\hat{\alpha})Y(\hat{\alpha})^{-2}$ . Now  $Y$  is a decreasing function of  $\alpha$ , while  $Q$  is increasing (see Appendix A.3). Hence  $c$  increases along the pattern solution branch as  $\hat{\alpha}$  increases from 1 (Hopf bifurcation) toward  $3/2$  (the homoclinic limit). Moreover,  $Y(3/2) = 0$ , while  $Q(3/2)$  is nonzero, so that  $c \rightarrow \infty$  in the homoclinic limit. The correct interpretation of this is that patterns exist for all values of  $A$  and  $c$  lying above the Hopf bifurcation curve  $A^2 = \frac{1}{2}B^2\nu c$  in the  $A$ - $c$  plane, and satisfying  $1/\nu \ll c \ll 1$  and  $A^2 = O_s(\nu c)$ . There is, of course, an upper boundary of the parameter region giving patterns, but it has  $c \gg 1$ .

**5.2. The cases  $\nu c \gg A^2 \gg 1/\nu c$  and  $A^2 = O_s(1/\nu c)$ .** Figure 5.1(a) shows the pattern solution for parameter values typical of the region considered in section 5.1. As  $A$  is decreased, the gently undulating profile for  $u$  changes into a spiked pattern (Figure 5.1(b)). Mathematically this is reflected by the pattern developing two different length scales. The spikes have width  $O_s(1)$  as  $\nu \rightarrow \infty$ , while their separation is  $O_s(\nu^{1/2}c^{1/2}/A)$ . The solution differs slightly in the two cases  $\nu c \gg A^2 \gg 1/\nu c$  and  $A = O_s(1/\nu c)$ , and I consider them together, commenting on differences as they arise.

I begin by considering the spikes. I substitute  $\bar{U}(z) = c^{-1/2}\nu^{-1/2}U(z)$  and  $\bar{W}(z) = c^{1/2}\nu^{1/2}W(z)$  into (1.2), giving

$$(5.1a) \quad \bar{U}'' + c\bar{U}' + \bar{W}\bar{U}^2 - B\bar{U} = 0,$$

$$(5.1b) \quad (\nu + c)\bar{W}' + \nu^{1/2}c^{1/2}A - \bar{W} - \nu c\bar{W}\bar{U}^2 = 0.$$

The appropriate expansions of the solutions are

$$(5.2) \quad \bar{U} = \bar{U}_0 + c\bar{U}_1 + \text{h.o.t.} \quad \text{and} \quad \bar{W} = \bar{W}_0 + c\bar{W}_1 + \text{h.o.t.}$$

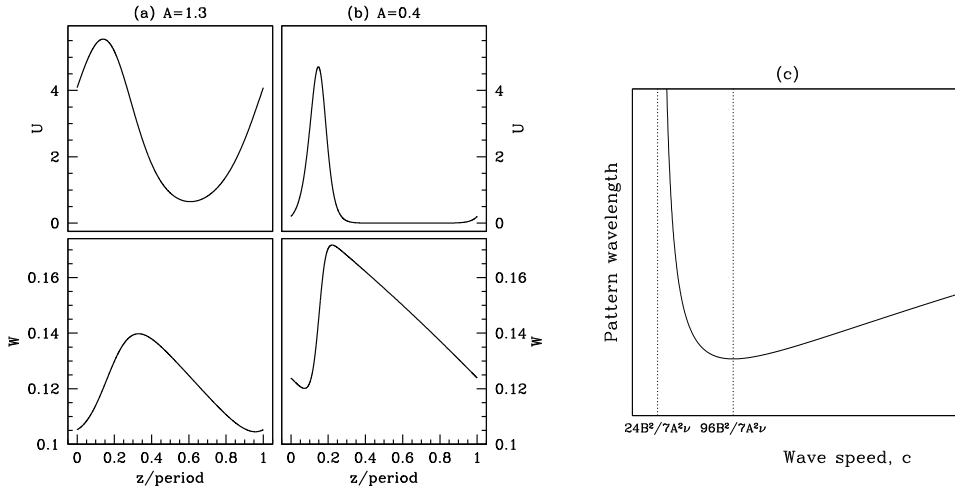


FIG. 5.1. (a) and (b) Two examples of pattern solutions of (1.1), plotted over one period (wavelength). The patterns in (a) and (b) are representative of those in the parameter regions studied in sections 5.1 and 5.2, respectively. The pronounced spike in  $u$  for (b) is reflected mathematically by the dependence of the solution on two different length scales, with different  $\nu$ -scalings. The parameter values are  $B = 0.45$ ,  $\nu = 200$ ,  $c = 0.15$ , and (a)  $A = 1.3$ , (b)  $A = 0.4$ . The patterns were calculated by numerical continuation along the branch of periodic solutions of (1.2), starting at the Hopf bifurcation point [30]. Numerical continuation was performed using the software package AUTO [28]. Note that the coordinate on the horizontal axis is the travelling wave coordinate divided by the period (wavelength), which is 13.0 for (a) and 49.8 for (b). (c) The variation in the leading order pattern wavelength with  $c$ , for fixed values of the other parameters, in the case  $A^2 = O_s(1/\nu c)$ . The wavelength is  $\bar{L}_0 A^{-1} c^{1/2} \nu^{1/2}$ , with  $\bar{L}_0$  given by (5.7). I have omitted tickmarks on the axes to emphasize the qualitative form, but this figure is a plot, not a sketch. The parameters are  $A = 0.3$ ,  $B = 0.45$ ,  $\nu = 200$ , and the axes ranges are  $0 \leq c \leq 0.5$  and  $700 \leq \text{wavelength} \leq 1800$ . The leading order approximation to the homoclinic limit,  $c = 24B^2/7A^2\nu$ , is 0.038. This is in good agreement with results from numerical simulation; for example, in Figure 2.1(a), which uses the same parameters, the relevant intersection of the homoclinic locus and the line  $A = 0.3$  occurs at  $c = 0.042$ .

The leading order solution of (5.1) is directly analogous to that in section 3:  $\bar{W}_0 = \bar{k}_0$  and  $\bar{U}_0 = (B/\bar{k}_0) U^*(B^{1/2}z; \bar{\alpha})$ , where  $\bar{\alpha} \in [1, 3/2]$  and  $\bar{k}_0$  are constants of integration.

Between the spikes, I write  $\bar{U}(\bar{z}) = c^{-1/2}\nu^{-1/2}U(z)$  and  $\bar{W}(\bar{z}) = c^{1/2}\nu^{1/2}W(z)$  with  $\bar{z} = Ac^{-1/2}\nu^{-1/2}z$ , giving

$$(5.3a) \quad A^2 c^{-1} \nu^{-1} \left( d^2 \bar{U} / d\bar{z}^2 \right) + Ac^{1/2} \nu^{-1/2} \left( d\bar{U} / d\bar{z} \right) + \bar{W} \bar{U}^2 - B \bar{U} = 0,$$

$$(5.3b) \quad \left( A\nu^{1/2} c^{-1/2} + A\nu^{-1/2} c^{1/2} \right) d\bar{W} / d\bar{z} + \nu^{1/2} c^{1/2} A - \bar{W} - \nu c \bar{W} \bar{U}^2 = 0.$$

The appropriate expansions are

$$(5.4) \quad \bar{U} = \bar{U}_0 + c\bar{U}_1 + \text{h.o.t.} \quad \text{and} \quad \bar{W} = \bar{W}_0 + c\bar{W}_1 + \text{h.o.t.}$$

To leading order, (5.3a) is  $\bar{W}_0 \bar{U}_0^2 - B \bar{U}_0 = 0$ . The possibility  $\bar{U}_0 \bar{W}_0 \equiv B$  gives a solution that matches at leading order, albeit with a form that differs qualitatively from numerical simulations such as those in Figure 5.1(b). However, for the resulting higher order terms, matching between the spike and interspike solutions is impossible

(details are omitted for brevity). Therefore  $\overline{U}_0 \equiv 0$ . Then the leading order solution for  $\overline{W}_0$  is a constant,  $\overline{W}_0 = \overline{k}_0$ .

Matching the spike and interspike solutions requires  $\overline{k}_0 = \overline{k}_0$  and  $\overline{U}_0(z) \rightarrow 0$  as  $z \rightarrow \pm\infty \Rightarrow \overline{\alpha} = 3/2$ . For this value of  $\overline{\alpha}$ ,  $U^*$  has the simple form  $U^*(\xi) = \frac{3}{2}\text{sech}^2(\xi/2)$ . The common value of  $\overline{k}_0$  and  $\overline{k}_0$  remains undetermined; this depends on higher order terms, which I now consider. In the interspike region, substituting (5.4) into (5.3) with  $\overline{U}_0 = 0$  implies that  $\overline{U}_1 = 0$ . The highest order undetermined terms in (5.3b) are then  $O_s(A\nu^{1/2}c^{1/2})$ , and the resulting equation for  $\overline{W}_1$  depends on the scaling for  $A$ :

$$(5.5a) \quad \nu c \gg A^2 \gg 1/\nu c : \quad d\overline{W}_1/d\overline{z} + 1 = 0 \quad \Rightarrow \overline{W}_1 = -\overline{z} + \overline{k}_1,$$

$$(5.5b) \quad A^2 = O_s(1/\nu c) : \quad d\overline{W}_1/d\overline{z} + 1 - \overline{k}_0/(A\nu^{1/2}c^{1/2}) = 0 \\ \Rightarrow \overline{W}_1 = \left(\overline{k}_0/(A\nu^{1/2}c^{1/2}) - 1\right)\overline{z} + \overline{k}_2,$$

where  $\overline{k}_1$  and  $\overline{k}_2$  are constants of integration.

For higher order terms in the spikes, I substitute (5.2) into (5.1b), giving

$$(5.6) \quad d\overline{W}_1/dz = \overline{W}_0\overline{U}_0^2 = (9B^2/4\overline{k}_0)\text{sech}^4\left(zB^{1/2}/2\right) \\ \Rightarrow \overline{W}_1 = \overline{k}_1 + (9B^{3/2}/2\overline{k}_0)\left[\tanh\left(zB^{1/2}/2\right) - \frac{1}{3}\tanh^3\left(zB^{1/2}/2\right)\right],$$

where  $\overline{k}_1$  is a constant of integration. In (5.1a), the highest order undetermined terms are  $O_s(c)$ ; using (5.6) and the solutions for  $\overline{U}_0$  and  $\overline{W}_0$ , one obtains an equation for  $\overline{U}_1$ , which can be solved in closed form by standard methods. However, the algebra is very involved, and I omit the details for brevity; a MAPLE worksheet that performs the various calculations is available in [31]. The solution has two constants of integration,  $\kappa_1$  and  $\kappa_2$  say. One of these,  $\kappa_1$  say, is determined by the condition  $\overline{U}_1'(0) = 0$ . For  $\kappa_2$  one must consider the condition  $\overline{U}_1 \rightarrow 0$  as  $z \rightarrow \pm\infty$ , which is required for matching with the interspike solution (recall that  $\overline{U}_0$  and  $\overline{U}_1$  are both identically zero). Asymptotic expansion of the solution for  $\overline{U}_1$  shows that  $\overline{U}_1 = \Upsilon_{\pm}(e^{\pm\sqrt{B}z} + 12) + o(1)$  as  $z \rightarrow \pm\infty$ , where  $\Upsilon_{\pm}$  are functions of  $\overline{k}_0$ ,  $\overline{k}_1$ ,  $B$ , and  $\kappa_2$ . Thus the matching conditions are satisfied  $\Leftrightarrow \Upsilon_+ = \Upsilon_- = 0$ . Solving these algebraic equations determines  $\kappa_2$  and implies that  $\overline{k}_0 = B\sqrt{24/7}$ .

There remains one outstanding aspect of the matched leading order solutions in the spike and interspike regions: the spike separation, which gives the leading order pattern wavelength. The scaling for this quantity mirrors that for  $\overline{z}$ , namely  $\overline{L}_0 A^{-1}c^{1/2}\nu^{1/2}$ , where  $\overline{L}_0 = O_s(1)$  as  $\nu \rightarrow \infty$ . To determine  $\overline{L}_0$ , I consider matching  $\overline{W}_0 + c\overline{W}_1$  and  $\overline{W}_0 + c\overline{W}_1$ . Since  $\overline{W}_0$  and  $\overline{W}_0$  are (equal) constants, I require  $\overline{W}_1(+\infty) = \overline{W}_1(\overline{z}_0)$  and  $\overline{W}_1(-\infty) = \overline{W}_1(\overline{z}_0 + \overline{L}_0)$  for some  $\overline{z}_0$ . Substituting (5.5), (5.6), and the expression for  $\overline{k}_0$  into these matching conditions gives

$$(5.7) \quad \nu c \gg A^2 \gg 1/\nu c : \quad \overline{L}_0 = \sqrt{21B/2}, \\ A^2 = O_s(1/\nu c) : \quad \overline{L}_0 = \sqrt{21B/2}(A\nu^{1/2}c^{1/2})\left(A\nu^{1/2}c^{1/2} - B\sqrt{24/7}\right)^{-1}.$$

Therefore for  $\nu c \gg A^2 \gg 1/\nu c$  (and  $1/\nu \ll c \ll 1$ ) there is always a pattern solution, and the leading order pattern wavelength  $\overline{L}_0 A^{-1}c^{1/2}\nu^{1/2}$  increases as  $A$  decreases.

For  $A^2 = O_s(1/\nu c)$  this trend continues, and the wavelength tends to infinity as the curve  $A^2 c = 24B^2/7\nu$  is approached. This homoclinic locus gives the lower limit on  $A$  for patterns, and its leading order form is the same as those calculated in sections 3 and 4. Figure 5.1(c) illustrates the variation in the leading order pattern wavelength with  $c$  in the case  $A^2 = O_s(1/\nu c)$ . Note in particular that the wavelength has a minimum at  $c = 96B^2/(7A^2\nu)$ . Intuitively, one can regard patterns above/below the curve  $A^2 c = 96B^2/7\nu$  as originating from a Hopf bifurcation of  $(u_+, w_+)/(u_-, w_-)$ . In section 3, I showed that when  $c = O_s(1/\nu)$  and  $A = O_s(1)$  with  $A < 2B$ , the wavelength decreases with  $\alpha$  and therefore its minimum is on  $A^2 c = 4B^2 Q(\alpha_{min})/\nu$ . As  $A/2B \rightarrow 0$ ,  $\alpha_{min} \rightarrow 3/2 \Rightarrow Q(\alpha_{min}) \rightarrow 24/7$ , so that the two results are in direct correspondence.

## 6. The instability of patterns with $c \ll 1$ .

**6.1. The cases  $c = O(1/\nu)$  and  $1/\nu \ll c \ll 1$ ,  $A^2 = O_s(\nu c)$ .** For the parameter regions studied in sections 3, 4, and 5.1, I showed that patterns have the form  $U = U^*(B^{1/2}z)$  with  $W$  constant, to leading order as  $\nu \rightarrow \infty$ . I now use this to show that these patterns are all unstable as solutions of (1.1) for sufficiently large  $\nu$ .

My argument regarding pattern stability is exactly the same for the three parameter regions corresponding to sections 3, 4, and 5.1, and I present it only for  $c = O_s(1/\nu)$ , corresponding to section 3. I begin by rewriting (1.1) using  $z$  and  $t$  rather than  $x$  and  $t$ , linearizing these equations about the pattern solution  $u = U(z)$ ,  $w = W(z)$ , and substituting  $u - U(z) = U_E(z)e^{\lambda t}$ ,  $w - W(z) = W_E(z)e^{\lambda t}$  into these linearized equations. Here  $\lambda \in \mathbb{C}$  is an eigenvalue and  $U_E(z), W_E(z) \in \mathbb{C}$  are the corresponding eigenfunctions. This gives

$$(6.1a) \quad \lambda U_E = U_E'' + cU_E' + 2UWU_E + U^2W_E - BU_E,$$

$$(6.1b) \quad \lambda W_E = (\nu + c)W_E' - W_E - 2UWU_E - U^2W_E.$$

For uniqueness, I fix the  $L_2$ -norm of  $(U_E, W_E)$  to be 1. The appropriate boundary condition is

$$(6.2) \quad (U_E(L), W_E(L)) = e^{i\gamma} (U_E(0), W_E(0)),$$

where  $L$  is the (minimal) period of the pattern  $(U, W)$ , and  $\gamma \in \mathbb{R}$  is arbitrary. Formally, this boundary condition can be derived using Floquet theory [32, 33]. Intuitively, the (complex-valued) components of the eigenfunction cannot change in amplitude across a period of the pattern; otherwise the eigenfunction would grow without bound on  $-\infty < z < \infty$ . Also the phase difference must be the same for  $U_E$  and  $W_E$  since they are coupled in (6.1), but otherwise it is unconstrained.

To show instability, it is sufficient to show that there is one eigenvalue with positive real part. I will show this for an eigenfunction for which  $W_E = o(1)$  as  $\nu \rightarrow \infty$ . Therefore I substitute

$$U = (B/k_0)U^*(B^{1/2}z) + o(1), \quad W = k_0 + o(1), \quad U_E = U_{E,0} + o(1), \quad \lambda = \lambda_0 + o(1)$$

into (6.1a) with  $W_E = o(1)$ , giving

$$(6.3) \quad \lambda_0 U_{E,0} = U_{E,0}'' + 2BU^*(B^{1/2}z)U_{E,0} - BU_{E,0}$$

to leading order as  $\nu \rightarrow \infty$ . I now make the substitutions

$$(6.4) \quad z = \frac{z^*}{\sqrt{B}}, \quad L = \frac{Z^*}{\sqrt{B}}, \quad U^* = \left(\frac{1}{2} - 6V\right)$$

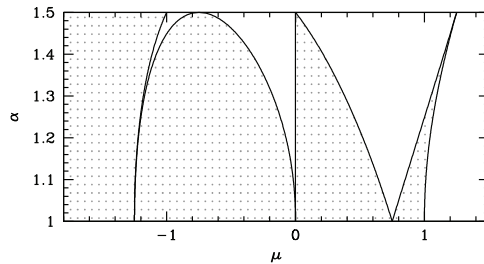


FIG. 6.1. Eigenvalues of Lamé's equation (6.7). The solid curves are the boundaries  $\mu_1, \mu_2, \dots, \mu_7$  of the intervals containing eigenvalues, which are indicated by gray spots. The curves were calculated using the method of Eilbeck and Enol'skii [37], which generates a seventh order polynomial whose roots are the  $\mu_i$ 's.

in (3.4) and (3.2), giving

$$(6.5) \quad \left( \frac{V(z^*)}{dz^*} \right)^2 = 4V^3 - \frac{1}{12}V - \frac{1}{216}(6\alpha^2 - 4\alpha^3 - 1),$$

$$(6.6) \quad V'(0) = 0, \quad V''(0) > 0.$$

Equation (6.5) is satisfied by the Weierstrass elliptic function  $\wp$  [34, Chapter 23], [35]. In general, this function is complex-valued, and the finite real-valued periodic solution satisfying (6.6) is  $V = \wp(z^* + i\Omega; g_2, g_3)$ . Here  $g_2 = \frac{1}{12}$  and  $g_3 = \frac{1}{216}(6\alpha^2 - 4\alpha^3 - 1)$  are the Weierstrass invariants, and  $Z^*$  and  $2\Omega i$  are the minimal periods ( $Z^*, \Omega \in \mathbb{R}$ ). Writing  $z^{**} = z^* + i\Omega$  and substituting (6.4) and  $\lambda_0 = B\mu$  into (6.2), (6.3) gives

$$(6.7) \quad d^2 U_{E,0} / dz^{**2} = 12\wp(z^{**})U_{E,0} + \mu U_{E,0},$$

$$(6.8) \quad U_{E,0}|_{z^{**}=i\Omega} = e^{i\gamma} U_{E,0}|_{z^{**}=Z^*+i\Omega} \quad (\gamma \in \mathbb{R} \text{ arbitrary}).$$

Equation (6.7) is Lamé's equation [34, Chapter 29], [36] with degree 3, for which the eigenvalues  $\mu$  are all real and consist of four (the degree plus 1) distinct intervals:  $(-\infty, \mu_1]$ ,  $[\mu_2, \mu_3]$ ,  $[\mu_4, \mu_5]$ , and  $[\mu_6, \mu_7]$  ( $\mu_1 < \mu_2 < \dots < \mu_7$ ). Figure 6.1 illustrates the dependence of the  $\mu_i$ 's on  $\alpha$ ; note that  $\mu_4 = 0$  for all  $\alpha$ , corresponding to the solution  $U_{E,0}(z^{**}) = \wp'(z^{**})$ . The key implication of these considerations is that two of the intervals containing eigenvalues lie in the right-hand half of the real line, and thus for any  $\alpha \in (1, 3/2)$  there is a continuum of possible positive values of  $\mu$ . Correspondingly, there are solutions of (6.3) with  $\lambda_0$  real and positive, and thus the pattern  $(U, W)$  is unstable for sufficiently large  $\nu$ .

**6.2. The case  $1/\nu \ll c \ll 1$ ,  $A^2 \ll \nu c$ .** I now consider pattern stability in the parameter region studied in section 5.2. I have shown that in this case, patterns consist of spikes whose width is  $O(1)$  as  $\nu \rightarrow \infty$ , but whose separations are  $O_s(\sqrt{\nu c}/A)$ , and in section 5.2 I constructed matched spike and interspike solutions. I will now show that these patterns are also all unstable for sufficiently large  $\nu$ . To do this, I will construct a corresponding matched eigenfunction corresponding to a real positive eigenvalue.

I take both the  $U$  and  $W$  components of my eigenfunction to be  $O_s(c)$  in the interspike region, so that it is sufficient to consider only the solution in the spike. Following the procedure in section 6.1, I rewrite (1.1) using  $z$  and  $t$ , linearize about the pattern solution  $u = c^{1/2}\nu^{1/2}\bar{U}(z)$ ,  $w = c^{-1/2}\nu^{-1/2}\bar{W}(z)$ , and substitute  $u -$

$c^{1/2}\nu^{1/2}\bar{U}(z) = \bar{U}_E(z)e^{\bar{\lambda}t}$ ,  $w - c^{-1/2}\nu^{-1/2}\bar{W}(z) = \bar{W}_E(z)e^{\bar{\lambda}t}$  into these linearized equations. This gives

$$(6.9a) \quad \bar{\lambda}\bar{U}_E = \bar{U}''_E + c\bar{U}'_E + 2\bar{U}\bar{W}\bar{U}_E + \nu c\bar{U}^2\bar{W}_E - B\bar{U}_E,$$

$$(6.9b) \quad \bar{\lambda}\bar{W}_E = (\nu + c)\bar{W}'_E - \bar{W}_E - 2\bar{U}\bar{W}\bar{U}_E - \nu c\bar{U}^2\bar{W}_E.$$

For uniqueness, I fix the  $L_2$ -norm of  $(\bar{U}_E, \bar{W}_E)$  to be 1.

I have shown in section 5.2 that  $\bar{W} = \bar{k}_0 + O(c)$  and  $\bar{U} = (3B/2\bar{k}_0)\operatorname{sech}^2(B^{1/2}z/2) + O(c)$ . Substituting these together with  $\bar{U}_E = \bar{U}_{E,0}(z) + O(c)$ ,  $\bar{W}_E = O(c)$ , and  $\bar{\lambda} = \bar{\lambda}_0 + O(c)$  into (6.9a) gives

$$(6.10) \quad \bar{\lambda}_0\bar{U}_{E,0} = \bar{U}''_{E,0} + 3B\operatorname{sech}^2(B^{1/2}z/2)\bar{U}_{E,0} - B\bar{U}_{E,0}.$$

I require that  $\bar{U}_{E,0}$  matches the  $O(1)$  part of the eigenfunction in the interspike region, which is zero; thus the appropriate boundary conditions are  $\bar{U}_{E,0} \rightarrow 0$  as  $z \rightarrow \pm\infty$ .

Equation (6.10) is exactly (6.3) with  $\alpha = 3/2$ , and it can therefore be converted to Lamé’s equation by substitutions equivalent to those used in section 6.1. At this limiting value of  $\alpha$ , Lamé’s equation reduces to Legendre’s equation [34, Chapter 14]. In fact, rewriting (6.10) using  $T = \tanh(B^{1/2}z/2)$  gives the standard form of Legendre’s equation. One can then exploit the known closed form solutions of this equation. In particular, the associated Legendre function  $P_3^3(T)$  corresponds to the solution  $\bar{U}_{E,0}(z) = \kappa \operatorname{sech}^3(B^{1/2}z/2)$  with  $\bar{\lambda}_0 = 5B/4$ , where the constant  $\kappa$  is determined by the normalization condition. This gives a leading order matched eigenfunction corresponding to a real positive eigenvalue, implying that the pattern  $(U, W)$  is unstable as a solution of (1.1).

**7. Small amplitude patterns for  $c = O_s(1)$ .** I now consider the case  $c = O_s(1)$  as  $\nu \rightarrow \infty$ . I will not attempt a comprehensive study of this parameter region. Rather, I will restrict myself to proving that for the leading order equations for large  $\nu$ , the small amplitude patterns in the immediate vicinity of the Hopf bifurcation locus are stable for some values of  $c$  and unstable for others.

For algebraic simplicity I make the substitutions

$$\check{u} = (B/A)u, \quad \check{w} = (A/B^2)w, \quad \check{x} = B^{1/2}x, \quad \check{t} = Bt, \quad \check{c} = B^{-1/2}c, \quad \Gamma = A^2/(\nu B^{5/2}).$$

In terms of these new variables, the leading order form of (1.1) as  $\nu \rightarrow \infty$  is

$$(7.1a) \quad \partial\check{u}/\partial\check{t} = \partial^2\check{u}/\partial\check{x}^2 + \check{w}\check{u}^2 - \check{u},$$

$$(7.1b) \quad 0 = \partial\check{w}/\partial\check{x} + \Gamma(1 - \check{w}\check{u}^2),$$

and the corresponding leading order travelling wave equations are

$$(7.2a) \quad d^2\check{U}/d\check{z}^2 + \check{c}d\check{U}/d\check{z} + \check{W}\check{U}^2 - \check{U} = 0,$$

$$(7.2b) \quad d\check{W}/d\check{z} + \Gamma(1 - \check{W}\check{U}^2) = 0,$$

where  $\check{u}(\check{x}, \check{t}) = \check{U}(\check{z})$  and  $\check{w}(\check{x}, \check{t}) = \check{W}(\check{z})$ ,  $\check{z} = \check{x} - \check{c}\check{t}$ . Equations (7.2) have a unique steady state  $\check{U} = \check{W} = 1$ , and calculation of the eigenvalues shows that for each  $\check{c} \in (0, \infty)$ , this steady state undergoes a Hopf bifurcation at exactly one value of  $\Gamma = \Gamma_H \equiv (\check{c}^2 + 2 - \sqrt{\check{c}^4 + 4})/(2\check{c})$ . Figure 7.1 illustrates the locus of these Hopf

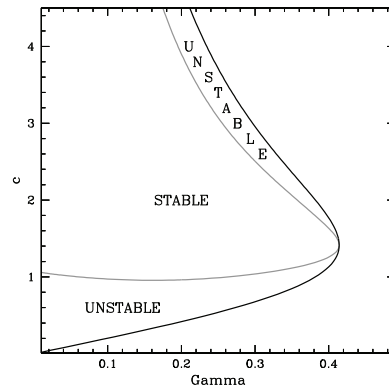


FIG. 7.1. Existence and stability of pattern solutions of (7.1). The black curve is the locus of Hopf bifurcation points of (7.2); patterns exist to the left of this curve. The gray curve is the boundary between stable and unstable patterns. These curves were calculated using the software package WAVETRAIN [30, 32, 38]. Full details of the WAVETRAIN input files, run commands, and plot commands are given in [31].

bifurcation points in the  $\Gamma$ - $\tilde{c}$  plane. Calculation of the normal form (see Appendix B) shows that at each point on this locus, the branch of limit cycles (patterns) leaves in the direction of decreasing  $\Gamma$ .

The main result of this section is the following.

**PROPOSITION.** For a given value of  $\tilde{c} \in \mathbb{R}^+$ , let  $\Gamma = \Gamma_H(\tilde{c}) - \delta(\tilde{c})$ . Then if  $\tilde{c} \neq \sqrt{2}$ , the small amplitude pattern solution of (7.2) is unstable as a solution of (7.1) for sufficiently small  $\delta$ , while for  $\tilde{c} = \sqrt{2}$  it is stable for sufficiently small  $\delta$ .

Figure 7.1 shows numerical results on the stability of periodic travelling wave solutions of (7.1), calculated using the software package WAVETRAIN [30]. These are in direct accord with the proposition. There is a curve in the  $\Gamma$ - $\tilde{c}$  plane separating stable and unstable solutions; this curve lies to the left of the Hopf bifurcation locus and touches it at  $\Gamma = \sqrt{2} - 1$ ,  $\tilde{c} = \sqrt{2}$ .

*Proof.* The eigenfunction equation governing pattern stability is

$$(7.3a) \quad \tilde{\lambda} \tilde{U}_E = d^2 \tilde{U}_E / d\tilde{z}^2 + \tilde{c} d\tilde{U}_E / d\tilde{z} + (2\tilde{U}\tilde{W} - 1)\tilde{U}_E + \tilde{U}^2 \tilde{W}_E,$$

$$(7.3b) \quad 0 = d\tilde{W}_E / d\tilde{z} - \Gamma (2\tilde{U}\tilde{W}\tilde{U}_E + \tilde{U}^2 \tilde{W}_E),$$

where  $(\tilde{U}_E, \tilde{W}_E)$  is the eigenfunction and  $\tilde{\lambda}$  is the corresponding eigenvalue. As discussed in section 6, the appropriate boundary condition is  $\tilde{U}_E(0) = e^{i\gamma} \tilde{U}_E(L)$ ,  $\tilde{W}_E(0) = e^{i\gamma} \tilde{W}_E(L)$ , with  $\gamma \in \mathbb{R}$  arbitrary. Since the Hopf bifurcation is non-degenerate (see Appendix B),  $\tilde{U} = 1 + o(\delta)$  and  $\tilde{W} = 1 + o(\delta)$  as  $\delta \rightarrow 0$ ; recall that  $\delta = \Gamma_H - \Gamma$ . I denote by  $\tilde{\lambda}_0$ ,  $\tilde{U}_{E,0}(\tilde{z})$ , and  $\tilde{W}_{E,0}(\tilde{z})$  the  $O_s(1)$  contributions to  $\tilde{\lambda}$ ,  $\tilde{U}_E(\tilde{z})$ , and  $\tilde{W}_E(\tilde{z})$  as  $\delta \rightarrow 0$ . Then to leading order as  $\delta \rightarrow 0$ , (7.3) becomes

$$(7.4a) \quad \tilde{\lambda}_0 \tilde{U}_{E,0} = d^2 \tilde{U}_{E,0} / d\tilde{z}^2 + \tilde{c} d\tilde{U}_{E,0} / d\tilde{z} + \tilde{U}_{E,0} + \tilde{W}_{E,0},$$

$$(7.4b) \quad 0 = d\tilde{W}_{E,0} / d\tilde{z} - \Gamma_H (2\tilde{U}_{E,0} + \tilde{W}_{E,0}).$$

There are three linearly independent solutions of (7.4), each proportional to  $e^{s\tilde{z}}$  with  $s$  being one of the three roots of

$$(7.5) \quad (s - \Gamma_H) (s^2 + \tilde{c}s + 1 - \tilde{\lambda}_0) + 2\Gamma_H = 0.$$

The boundary conditions require  $s$  to be purely imaginary, say  $s = iq$  with  $q \in \mathbb{R}$ . Using this and eliminating  $\text{Im } \check{\lambda}_0$  between the real and imaginary parts of (7.5) gives

$$(7.6) \quad \text{Re } \check{\lambda}_0 = \frac{(\Gamma_H^4 - 6\Gamma_H^2 + 1) - (2q^2 + \Gamma_H^2 - 1)^2}{4(\Gamma_H^2 + q^2)}.$$

Now the pattern is unstable for sufficiently small  $\delta$  if  $\text{Re } \check{\lambda}_0 > 0$  for any  $q \in \mathbb{R}$ , i.e., if

$$0 < \Gamma_H^4 - 6\Gamma_H^2 + 1 = \left(\sqrt{2} - 1 - \Gamma_H\right) \left(\sqrt{2} + 1 - \Gamma_H\right) \left(\Gamma_H^2 + 2\sqrt{2}\Gamma_H + 1\right).$$

Now  $\Gamma_H(\check{c}) > 0$  with a unique local maximum at  $\check{c} = \sqrt{2}$ ,  $\Gamma_H = \sqrt{2} - 1$ . Therefore the pattern is unstable, for sufficiently small  $\delta$ , if  $\check{c} \neq \sqrt{2}$ .

When  $\check{c} = \sqrt{2}$ ,  $\text{Re } \check{\lambda}_0 \leq 0$  for all  $q$ . No conclusion can be drawn from this about the stability of the pattern for small  $\delta$ : since  $\text{Re } \check{\lambda}_0$  becomes zero as  $q$  is varied, stability will depend on  $O(\delta)$  contributions to  $\check{\lambda}$ . To investigate stability in this case, I adopt a different approach. I consider stability of the steady state  $\check{u} = \check{w} = 1$  of (7.1). Linearizing (7.1) about this steady state and using the solution ansatz  $(\check{u} - 1, \check{w} - 1) \propto \exp(\Lambda t + i\check{k}\check{x})$  yields the dispersion relation

$$\text{Re } \Lambda = \left[ \Gamma^4 - 6\Gamma^2 + 1 - (2\check{k}^2 + \Gamma^2 - 1)^2 \right] / [4(\Gamma^2 + \check{k}^2)].$$

Therefore  $(\check{u}, \check{w}) = (1, 1)$  changes stability when  $\Gamma^4 - 6\Gamma^2 + 1 = 0$ , with the associated wavenumber being  $\check{k} = [(1 - \Gamma^2)/2]^{1/2} \Rightarrow \Gamma < 1$ . Thus stability is lost as  $\Gamma$  decreases through  $\sqrt{2} - 1$ . As expected, this is exactly the value of  $\Gamma$  at which  $\Gamma_H(\check{c})$  has its maximum; for (7.1) it is a Turing bifurcation point. Moreover, the fact that the limit cycle branches of (7.2) leave the Hopf bifurcation locus in the direction of decreasing  $\Gamma$  (see Appendix B) implies that the Turing bifurcation is supercritical. General theory (e.g., [39, 40]) then implies that (7.1) has stable small amplitude patterns for  $\Gamma$  below and sufficiently close to the Turing bifurcation value of  $\sqrt{2} - 1$ . This completes the proof of the proposition.  $\square$

**8. Discussion.** The upslope migration of banded vegetation is a major controversy dating back to the first reports of these patterns in Africa in the 1950s and '60s. The evidence for migration of some of these patterns is extremely strong. This includes measurements of pattern location relative to ground benchmarks [41, 42] and indirect measures such as differences in seedling density and plant death on the upslope and downslope sides of the bands [22, 24, 43], and the use of radioactive isotopes to determine soil dynamics [44, 45]. However, there is also compelling evidence that other banded vegetation patterns are static, again involving both direct data [4, 46] and indirect measures [6, 25]. An important contribution to this debate comes from the recent Ph.D. thesis of Deblauwe [23], which makes a careful comparison between recent satellite images and those from the 1960s and '70s; declassified spy satellite images are an important source for the older data. This work revealed very clear evidence of upslope migration in three cases, but no evidence of migration at three other sites.

One natural potential explanation for pattern migration being detected at some locations and not at others is that in the latter, migration speeds are simply too low to be detectable over time scales of a few decades. This would require migration speeds that are at least an order of magnitude less than values recorded in direct measurements (0.3–0.8 m/year [23, 41, 42]). For the Klausmeier model (1.1), previous numerical bifurcation studies have shown that pattern solutions with very low

speeds do exist [27] (see Figure 2.1(a)). However, in this paper I have shown that these very slowly moving patterns are unstable as solutions of the model equations (1.1). Moreover, I have shown in section 6 that this instability is associated with an eigenvalue of real part at least  $B$ . Using the nondimensionalization and parameter estimates of Klausmeier [7], the corresponding dimensional doubling time for perturbations ( $\log 2/4B$  years) is between 5 months and 4 years depending on vegetation type, which is significantly less than the time scale (decades) over which some patterns are stationary in the field. This argues strongly for a dominant role being played by an additional factor that is not included in the Klausmeier model. One possibility for this factor is changes in soil structure. The continual water run-off in the interbands causes a gradual loss of materials, which are deposited on the uphill side of the vegetation bands. This leads to hard, dense soils immediately above the bands, which inhibit seed germination [4]. Another possibility is that seed dispersal may be preferentially oriented in the downslope direction, due to transport in run-off [47]. Thompson and Katul [48] developed mathematical models that incorporate this “secondary seed dispersal” and demonstrated stationary vegetation patterns in model simulations.

The pattern solutions of (1.1) are periodic travelling waves (PTWs). For most systems, PTWs can be studied only numerically [30]. For the Klausmeier model (1.1), I have obtained a complete analytical description of the PTWs with  $c \ll 1/\nu$ , to leading order for large  $\nu$ . This includes explicit formulae for the rainfall range over which there are PTWs. My results are formal, and a natural area for future work is to attempt to establish them rigorously, for example, using geometric singular perturbation theory [19, 20, 21]. An analytical calculation of PTWs is very unusual; other examples include the piecewise constant Fitzhugh–Nagumo equation [49],  $\lambda$ - $\omega$  reaction-diffusion systems [50], and the complex Ginzburg–Landau equation [51]. The latter two cases are the only examples for which I am aware of previous analytical results on PTW stability. In both of these cases, stability reduces to an algebraic eigenvalue problem because the equations can be rewritten using the solution amplitude and phase gradient as variables; the PTW solutions then become homogeneous equilibria.

The fact that all of the PTWs of (1.1) with  $c = o(1)$  as  $\nu \rightarrow \infty$  are unstable precludes uninterrupted expanses of the patterns. However, it does not mean that the solutions are entirely irrelevant in applications. General theory of PTW stability [33, 52] implies that the parameter region giving unstable waves will subdivide into waves that are absolutely unstable and those that are only convectively unstable. The latter parameter region is typically adjacent to that giving stable waves and corresponds to all unstable linear modes being mobile; absolute instability means the existence of stationary unstable linear modes. Convectively unstable PTWs can be permanent features of PDE solutions, appearing as long-term spatiotemporal transients [53, 54, 55]. It is only below the absolute stability threshold that PTWs will never be seen as a component of the solution. Even then, a knowledge of the PTW solutions can be helpful in understanding the observed spatiotemporal dynamics [56]. Calculation of the boundary in parameter space between convectively and absolutely unstable patterns for (1.1) is currently out of reach, even numerically [32], and is an important challenge for future research.

**Appendix A.** In this appendix, I give the details of various calculations that underlie my investigation of the form and existence of patterns for  $c = O_s(1/\nu)$ . For notational simplicity, I write  $L_0\sqrt{B}/2 = \ell$ , and I define  $I_n = \int_{-\ell}^{\ell} U^*(\xi)^n d\xi$  ( $n \in \mathbb{N}$ ); thus  $I_0 = L_0\sqrt{B}$ .

**A.1. Derivation of (3.8).** Equation (3.3)  $\Rightarrow U_0'(2k_0U_0 - B) = -U_0'''$ . Multiplying (3.7) through by  $U_0'$  therefore gives

$$(A.1) \quad CU_0'^2 + W_1U_0^2U_0' = U_0'''U_1 - U_0'U_1'' = (U_0''U_1 - U_0'U_1')'$$

Periodicity of  $U_1$  requires

$$[U_0(z) + \nu^{-1}U_1(z)]_{z=-(L_0+\nu^{-1}L_1)/2}^{z=(L_0+\nu^{-1}L_1)/2} = O(\nu^{-2}) \Rightarrow [U_1(z)]_{z=-L_0/2}^{z=L_0/2} = -L_1U_0'(L_0/2).$$

Similarly,  $U_1'(L_0/2) - U_1'(-L_0/2) = -L_1U_0''(L_0/2)$ . Since  $U_0$  and its derivatives are periodic with period  $L_0$ , it follows that  $U_0''U_1 - U_0'U_1'$  has the same value at  $z = \pm L_0/2$ , and thus integrating (A.1) between  $-L_0/2$  and  $L_0/2$  gives

$$(A.2) \quad C = - \int_{z=-L_0/2}^{z=L_0/2} W_1(z)U_0^2(z)U_0'(z)dz \Big/ \int_{z=-L_0/2}^{z=L_0/2} U_0'^2(z)dz.$$

The solution for  $W_1$  is given by integrating (3.5); (A.2) is independent of the constant of integration, and

$$(A.3) \quad \begin{aligned} \int_{-L_0/2}^{L_0/2} W_1U_0^2U_0' &= (k_0 - A)k_0^{-3}B^{5/2} \int_{-\ell}^{\ell} \xi U^*(\xi)^2 U^{*'}(\xi) d\xi \\ &+ B^{9/2}k_0^{-4} \int_{\xi=-\ell}^{\xi=\ell} U^*(\xi)^2 U^{*'}(\xi) \int_{\zeta=0}^{\zeta=\xi} U^*(\zeta)^2 d\zeta d\xi \quad \text{using (3.3)} \\ &= B^{9/2}k_0^{-4} (Y(\alpha)\mathcal{T}_1 + \mathcal{T}_2) \quad \text{using (3.6),} \end{aligned}$$

$$(A.4) \quad \text{where } \mathcal{T}_1 = - \int_{-\ell}^{\ell} \xi \left( \frac{d}{d\xi} \right) \left[ \frac{1}{3}U^*(\xi)^3 \right] d\xi = \frac{1}{3} (I_3 - \beta^3 I_0)$$

$$(A.5) \quad \text{and } \mathcal{T}_2 = \int_{\xi=-\ell}^{\xi=\ell} \int_{\zeta=0}^{\zeta=\xi} U^*(\xi)^2 d\zeta d\xi = \frac{1}{3}(\beta^3 I_2 - I_5).$$

In simplifying the formulae for  $\mathcal{T}_1$  and  $\mathcal{T}_2$ , I use  $U^*(\pm\ell) = \beta$ . I now consider the denominator in (A.2):

$$(A.6) \quad \left( k_0^2/B^{5/2} \right) \int_{z=-L_0/2}^{z=L_0/2} U_0'(z)^2 dz = \int_{-\ell}^{\ell} U^{*'}(\xi)^2 d\xi = \left[ \left( \frac{2}{3}\alpha^3 - \alpha^2 \right) I_0 - \frac{2}{3}I_3 + I_2 \right]$$

using (3.4). Differentiating (3.4) and multiplying through by  $U^{*n}$  gives

$$(A.7) \quad \begin{aligned} &U^{*n}U^{*''} + U^{*n+2} - U^{*n+1} = 0 \\ \Rightarrow &\left( U^{*n}U^{*'} \right)' - nU^{*n-1} \left( \frac{2}{3}\alpha^3 - \alpha^2 - \frac{2}{3}U^{*3} + U^{*2} \right) + U^{*n+2} - U^{*n+1} = 0 \\ \Rightarrow &(2n + 3)I_{n+2} - (3n + 3)I_{n+1} - (2\alpha^3 - 3\alpha^2)nI_{n-1} = 0. \end{aligned}$$

This recurrence relation enables  $I_3, I_4$ , and  $I_5$  to be expressed in terms of  $I_0 = L_0\sqrt{B}$ ,  $I_1$ , and  $I_2$ . Also (3.4) implies immediately that  $I_1 = I_2$ . This enables (A.3)–(A.6) to be combined and simplified to give (3.8), using  $Y = I_1/I_0$ .

**A.2. Behavior as  $\alpha \rightarrow 1^+$  and  $\alpha \rightarrow \frac{3}{2}^-$ .** As  $\alpha \rightarrow 1^+$ , the amplitude of  $U^*$  decreases to zero  $\Rightarrow I_1 - I_0 \rightarrow 0 \Rightarrow Y \rightarrow 1$ . The value of  $Q(1)$  can be found by calculating the leading order term in  $Y(\alpha) - 1$  as  $\alpha \rightarrow 1^+$ . However, the algebra

is rather involved, and a simpler argument is available, as follows. When  $A \geq 2B$ , the steady states  $(u_{\pm}, w_{\pm})$  in (1.2) undergo a Hopf bifurcation at the values of  $C$  given in (2.2b), (2.2c). Since  $\alpha = 1$  at the bifurcation point, (3.8) implies that the corresponding values of  $C$  must equal  $(B/k_0|_{\alpha=1})^2 Q(1)$ , with the two different values in (2.2b), (2.2c) corresponding to the two roots of (3.6) for  $k_0$ . From (3.6), it follows that  $Q(1) = 2$ .

I now consider behavior as  $\alpha \rightarrow \frac{3}{2}^-$  on the solution branch corresponding to the larger root of (3.6) for  $k_0$ , focusing on the direction of approach of  $C$  to its limiting value  $C_{\text{hc}}$ . The function  $U^*(\xi)$  is monotonic for  $\xi \in (-L_0\sqrt{B}/2, 0)$ . Therefore the integration variable in  $I_2$  can be changed from  $\xi$  to  $U^*$ , giving

$$I_2|_{\alpha=3/2} = 2 \int_0^{3/2} U^* (1 - \frac{2}{3}U^*)^{-1/2} dU^* = (9/2) \int_0^1 \tau(1-\tau)^{-1/2} d\tau = 6.$$

Denoting by  $K$  the complete elliptic integral of the first kind [29, section 3.131.5], (3.3), (3.4) give

$$(A.8) \quad L_0 = \left( \frac{48}{(4\alpha + 2\beta - 3)B} \right)^{1/2} K \left( \sqrt{\frac{2\alpha - 2\beta}{4\alpha + 2\beta - 3}} \right).$$

Standard references (e.g. [34, section 19.12.1]) give the asymptotic behavior of  $K$  as its argument approaches 1, which implies  $I_0 = B^{1/2}L_0 = -\log(\frac{3}{2} - \alpha) + O(1)$  as  $\alpha \rightarrow \frac{3}{2}^-$ . Therefore  $Y \equiv I_2/I_0 \sim -6/\log(\frac{3}{2} - \alpha)$  as  $\alpha \rightarrow \frac{3}{2}^-$ . Substituting this into (3.8) gives

$$(A.9) \quad Q(\alpha) = \left( \frac{24}{7} \right) + 12/\log \left( \frac{3}{2} - \alpha \right) + \text{h.o.t.}$$

as  $\alpha \rightarrow \frac{3}{2}^-$ . The larger root of (3.6) is

$$(A.10) \quad k_0 = \frac{A}{2} + \sqrt{\frac{A^2}{4} - B^2 Y} = A + 6 \left( \frac{B^2}{A} \right) / \log \left( \frac{3}{2} - \alpha \right) + \text{h.o.t.}$$

Substituting (A.9) and (A.10) into (3.8) implies

$$C = \frac{24B^2}{7A^2} + \frac{12B^2}{A^2} \left( 1 - \frac{24B^2}{7A^2} \right) / \log \left( \frac{3}{2} - \alpha \right) + \text{h.o.t.}$$

It follows that as  $\alpha \rightarrow \frac{3}{2}^-$ ,  $C$  approaches  $C_{\text{hc}} = 24B^2/(7A^2)$  from below if  $24B^2 > 7A^2$ , and from above otherwise. Finally, comparison of  $C_{\text{hc}}$  with  $C_{\text{hopf}} = 1/2[(A/B) - \{(A/B)^2 - 4\}^{1/2}]^2$  (see (2.2b)) shows that  $C_{\text{hc}} < C_{\text{hopf}} \Leftrightarrow A < [6B/(2\sqrt{21} - 7)]$ .

**A.3. Monotonicity of  $L_0$ ,  $Y$ , and  $Q$ .** The plots in Figure 3.1 suggest that  $L_0$ ,  $Y$ , and  $Q$  are increasing, decreasing, and increasing functions of  $\alpha$ , respectively. To consider this in detail it is helpful to use  $U^*(\xi) = \frac{1}{2} - 6\wp(\xi + i\Omega; g_2, g_3)$ , which follows from (6.4, 6.5, 6.6). I denote by  $2\omega$  and  $2\Omega i$  the minimal periods of  $\wp(\cdot)$  ( $\omega, \Omega \in \mathbb{R}$ ). Thus  $L_0 = 2\omega B^{1/2}$ . The Weierstrass invariants are  $g_2 = \frac{1}{12}$  and  $g_3 = \frac{1}{216}(2\psi - 1)$ , where  $\psi = 3\alpha^2 - 2\alpha^3$ ; these imply that the discriminant  $g_2^3 - 27g_3^2 = \psi(1 - \psi)/432$ . Since I am considering  $\alpha \in (1, \frac{3}{2})$ , it follows that  $\psi \in (0, 1)$  and that the discriminant is strictly positive. The Weierstrass eta-function  $\eta$  is defined by

$\eta = -\frac{1}{2} \int_{x_0=0}^{x_0=2\omega} \wp(x_0 + z_0) dx_0$ , which is independent of  $z_0 \in \mathbb{C}$  [34, sections 23.2.7 and 23.2.11]. Thus  $I_1 = \omega + 12\eta$ , while  $I_0 = 2\omega$ , implying  $Y(\alpha) = \frac{1}{2} + 6\eta/\omega$ .

Formulae for  $\partial\omega/\partial g_3$  and  $\partial\eta/\partial g_3$  can be obtained using the approach of [57]. Using these, one obtains the following, after considerable algebraic simplification:

$$(A.11a) \quad \frac{dL_0}{d\alpha} = \frac{\alpha(\alpha-1)(Y-\psi)L_0}{\psi(1-\psi)},$$

$$(A.11b) \quad \frac{dY}{d\alpha} = \frac{-\alpha(\alpha-1)[Y(Y-\psi) + \psi(1-Y)]}{\psi(1-\psi)},$$

$$(A.11c) \quad \frac{dQ}{d\alpha} = \frac{2\alpha(\alpha-1)\mathcal{D}}{7(Y-\psi)^2\psi(1-\psi)},$$

where  $\mathcal{D} = 7Y^4 - 28\psi Y^3 - (35\psi^2 - 77\psi)Y^2 + (6\psi^3 + 26\psi^2 - 60\psi)Y + 10\psi^2 - 3\psi^3$ . Integrating (3.4) over one period and using (A.7) gives  $Y - \psi = (5/I_0) \int_{-I_0/2}^{I_0/2} U^{*'}{}^2 > 0$ . Therefore  $Y > \psi$ ; also  $\alpha > 1$  and  $\psi \in (0, 1)$ . Hence  $dL_0/d\alpha > 0$ . Now  $Y \rightarrow 1$  as  $\alpha \rightarrow 1^+$ , since  $\alpha = 1$  is the Hopf bifurcation limit at which  $U^* \equiv 1$ . Asymptotic expansions of  $U^*$  and  $I_0$  show further that, for  $\alpha - 1$  strictly positive and sufficiently small,  $Y < 1$ ; details of this calculation are omitted for brevity but are given in [31]. From (A.11b) it follows that  $dY/d\alpha < 0$  for  $\alpha - 1$  small and positive, and thus  $Y$  remains  $< 1$  as  $\alpha$  increases, so that  $dY/d\alpha$  remains negative.

For  $Q$ , (A.11c) implies that  $dQ/d\alpha$  has the same sign as  $\mathcal{D}$ . I have been unable to show analytically that  $\mathcal{D} > 0$  throughout the solution, but (A.11) enables a very robust numerical demonstration. Equation (A.11b) can be solved with very high accuracy to determine  $Y(\alpha)$ ; this approach offers much better error control than the direct evaluation of the integrals  $I_0$  and  $I_1$  that was used for Figure 3.1. A starting point is required for the numerical solution, and the end points  $\alpha = 1$  and  $\alpha = 3/2$  are both unsuitable, being singularities for (A.11b). Fortunately a suitable interior starting point is available, namely  $\alpha = (1 + \sqrt{3})/2$ . This gives  $\psi = 1/2 \Rightarrow g_3 = 0$ , which is the ‘‘lemniscatic’’ case of  $\wp(\cdot)$ , for which exact formulae for  $\omega$  and  $\eta$  are available [34, sections 23.5.2 and 23.5.4]. Using these, one obtains  $Y((1 + \sqrt{3})/2) = \frac{1}{2} + \sqrt{3}\Gamma(3/4)^4/(2\pi^2)$ . I solved (A.11b) numerically from this starting point, for both increasing and decreasing  $\alpha$ . Throughout the integration, I monitored the value of  $\mathcal{D}$ ; it remains positive throughout  $1 < \alpha < 3/2$ . Hence  $dQ/d\alpha > 0$ .

**Appendix B.** In section 7, I stated that in (7.2), the branch of pattern solutions emanating from any point on the locus of Hopf bifurcations leaves that point in the direction of decreasing  $\Gamma$ . In this appendix, I give details of the calculations on which this statement is based. My discussion will be deliberately brief; a MAPLE worksheet that performs the various calculations is available in [31].

Recall that (7.2) has a unique equilibrium  $\check{U} = \check{W} = 1$ , which has exactly one Hopf bifurcation as  $\Gamma$  is varied, for any given value of  $c$ . Algebraically, it is most convenient to replace the parameter  $c$  by the imaginary part  $\omega \in (0, 1)$  of the purely imaginary eigenvalues at this Hopf bifurcation point; the appropriate substitution is  $c = \sqrt{1 - \omega^4}/\omega$ , and the Hopf bifurcation locus is then  $\Gamma = \Gamma_H \equiv \omega\sqrt{1 - \omega^4}/(1 + \omega^2)$ . I denote by  $\mu(\Gamma, \omega)$  the eigenvalue that is equal to  $i\omega$  at  $\Gamma = \Gamma_H$ . Consider now  $\Gamma = \Gamma_H + \varepsilon$ ; then  $\mu = i\omega + \varepsilon\partial\mu/\partial\Gamma|_{\Gamma=\Gamma_H} + O(\varepsilon^2)$  as  $\varepsilon \rightarrow 0$ . Substituting these into the characteristic equation and equating coefficients of  $\varepsilon$  shows that

$$\left. \frac{\partial \operatorname{Re} \mu}{\partial \Gamma} \right|_{\Gamma=\Gamma_H} = \frac{1 + \omega^2 + \omega^4 + \omega^6}{2(1 - \omega^2 + \omega^4 + \omega^6)},$$

which is  $> 0$  for all  $\omega \in (0, 1)$ . Therefore the real part of the complex conjugate pair of eigenvalues changes from negative to positive as  $\Gamma$  increases through  $\Gamma_H$ .

It is now necessary to determine whether the Hopf bifurcation is subcritical or supercritical. This involves a standard though somewhat laborious calculation of the first Lyapunov coefficient  $l_1(0)$  for the Hopf bifurcation<sup>1</sup> [58, 59], which gives

$$(B.1) \quad l_1(0) = \frac{\sqrt{1 - \omega^4} \left[ 36\omega^6 (20\omega^4 + 20\omega^2 + 9) + (2\omega^2 + 1) \left( (18\omega^2 - 5)^2 + 11 \right) \right]}{72(3 - \omega^2)(1 - \omega^2 + 4\omega^4 + 4\omega^6)(1 - \omega^2 + \omega^4 + \omega^6)}.$$

Therefore  $l_1(0) > 0$  for all  $\omega \in (0, 1)$ , implying that the Hopf bifurcation is subcritical. Therefore the pattern (limit cycle) solution branch leaves the Hopf bifurcation point in the direction in which  $\text{Re } \mu > 0$ , i.e., in the direction of decreasing  $\Gamma$ .

**Acknowledgments.** I am very grateful to Yurii Brezhnev, Chris Eilbeck, Matthew England, and Peter Walker for helpful discussions.

#### REFERENCES

- [1] C. VALENTIN, J. M. D'HERBÈS, AND J. POESEN, *Soil and water components of banded vegetation patterns*, *Catena*, 37 (1999), pp. 1–24.
- [2] M. RIETKERK, S. C. DEKKER, P. C. DE RUITER, AND J. VAN DE KOPPEL, *Self-organized patchiness and catastrophic shifts in ecosystems*, *Science*, 305 (2004), pp. 1926–1929.
- [3] W. MACFADYEN, *Vegetation patterns in the semi-desert plains of British Somaliland*, *Geographical J.*, 116 (1950), pp. 199–211.
- [4] D. L. DUNKERLEY AND K. J. BROWN, *Oblique vegetation banding in the Australian arid zone: Implications for theories of pattern evolution and maintenance*, *J. Arid Environ.*, 52 (2002), pp. 163–181.
- [5] A. K. McDONALD, R. J. KINUCAN, AND L. E. LOOMIS, *Ecohydrological interactions within banded vegetation in the northeastern Chihuahuan Desert, USA*, *Ecohydrology*, 2 (2009), pp. 66–71.
- [6] P. COUTERON, A. MAHAMANE, P. OUEDRAOGO, AND J. SEGHERI, *Differences between banded thickets (tiger bush) at two sites in West Africa*, *J. Veg. Sci.*, 11 (2000), pp. 321–328.
- [7] C. A. KLAUSMEIER, *Regular and irregular patterns in semiarid vegetation*, *Science*, 284 (1999), pp. 1826–1828.
- [8] J. A. SHERRATT, *An analysis of vegetation stripe formation in semi-arid landscapes*, *J. Math. Biol.*, 51 (2005), pp. 183–197.
- [9] M. RIETKERK, M. C. BOERLIJST, F. VAN LANGEVELDE, R. HILLERISLAMBERS, J. VAN DE KOPPEL, L. KUMAR, H. H. PRINS, AND A. M. DE ROOS, *Self-organization of vegetation in arid ecosystems*, *Am. Nat.*, 160 (2002), pp. 524–530.
- [10] E. GILAD, J. VON HARDENBERG, A. PROVENZALE, M. SHACHAK, AND E. MERON, *A mathematical model of plants as ecosystem engineers*, *J. Theoret. Biol.*, 244 (2007), pp. 680–691.
- [11] N. URSINO, *Above and below ground biomass patterns in arid lands*, *Ecol. Model.*, 220 (2009), pp. 1411–1418.
- [12] V. GUTTAL AND C. JAYAPRAKASH, *Self-organization and productivity in semi-arid ecosystems: Implications of seasonality in rainfall*, *J. Theoret. Biol.*, 248 (2007), pp. 490–500.
- [13] J. VAN DE KOPPEL, M. RIETKERK, F. VAN LANGEVELDE, L. KUMAR, C. A. KLAUSMEIER, J. M. FRYXELL, J. W. HEARNE, J. VAN ANDEL, N. DE RIDDER, A. SKIDMORE, L. STROOSNIJDER, AND H. H. PRINS, *Spatial heterogeneity and irreversible vegetation change in semiarid grazing systems*, *Am. Nat.*, 159 (2002), pp. 209–218.
- [14] R. LEFEVER, N. BARBIER, P. COUTERON, AND O. LEJEUNE, *Deeply gapped vegetation patterns: On crown/root allometry, criticality and desertification*, *J. Theoret. Biol.*, 261 (2009), pp. 194–209.
- [15] J. A. SHERRATT, *Pattern solutions of the Klausmeier model for banded vegetation in semi-arid environments I*, *Nonlinearity*, 23 (2010), pp. 2657–2675.

<sup>1</sup>I calculated  $l_1(0)$  using the formula in [59], which involves the eigenvector corresponding to the eigenvalue  $i\omega$  at the Hopf bifurcation point. The resulting value of  $l_1(0)$  (though not its sign) depends on the normalization chosen for the eigenvector. Formula (B.1) is for the eigenvector having a 2-norm of 1.

- [16] J. A. SHERRATT, *Pattern solutions of the Klausmeier model for banded vegetation in semi-arid environments II: Patterns with the largest possible propagation speeds*, Proc. R. Soc. A, 467 (2011), pp. 3272–3294.
- [17] J. A. SHERRATT, *Pattern solutions of the Klausmeier model for banded vegetation in semi-arid environments III: The transition between homoclinic solutions*, Phys. D, 242 (2013), pp. 30–41.
- [18] Y. GOTO, D. HILHORST, E. MERON, AND R. TEMAM, *Existence theorem for a model of dryland vegetation*, Discrete Contin. Dyn. Syst. Ser. B, 16 (2011), pp. 197–224.
- [19] C. K. R. T. JONES, *Geometric singular perturbation theory*, in Dynamical Systems, Lecture Notes in Math. 1609, R. Johnson, ed., Springer-Verlag, Berlin, 1995, pp. 44–118.
- [20] A. DOELMAN, T. J. KAPER, AND P. A. ZEGELING, *Pattern formation in the one-dimensional Gray-Scott model*, Nonlinearity, 10 (1997), pp. 523–563.
- [21] P. VAN HELJSTER AND B. SANDSTEDTE, *Planar radial spots in a three-component FitzHugh-Nagumo system*, J. Nonlinear Sci., 21 (2011), pp. 705–745.
- [22] D. J. TONGWAY AND J. A. LUDWIG, *Theories on the origins, maintenance, dynamics, and functioning of banded landscapes*, in Banded Vegetation Patterning in Arid and Semi-arid Environments, D. J. Tongway, C. Valentin, and J. Seghieri, eds., Springer, New York, 2001, pp. 20–31.
- [23] V. DEBLAUWE, *Modulation des structures de végétation auto-organisées en milieu aride*, Ph.D. thesis, Université Libre de Bruxelles, Brussels, Belgium, 2010; available online at <http://theses.ulb.ac.be/ETD-db/collection/available/ULBetd-04122010-093151/>.
- [24] C. MONTAÑA, J. SEGHERI, AND A. CORNET, *Vegetation dynamics: Recruitment, regeneration in two-phase mosaics*, in Banded Vegetation Patterning in Arid and Semi-arid Environments, D. J. Tongway, C. Valentin, and J. Seghieri, eds., Springer, New York, 2001, pp. 132–145.
- [25] J. A. MABBUTT AND P. C. FANNING, *Vegetation banding in arid Western Australia*, J. Arid Environ., 12 (1987), pp. 41–59.
- [26] A. I. BORTHAGARAY, M. A. FUENTES, AND P. A. MARQUET, *Vegetation pattern formation in a fog-dependent ecosystem*, J. Theoret. Biol., 265 (2010), pp. 18–26.
- [27] J. A. SHERRATT AND G. J. LORD, *Nonlinear dynamics and pattern bifurcations in a model for vegetation stripes in semi-arid environments*, Theor. Popul. Biol., 71 (2007), pp. 1–11.
- [28] E. J. DOEDEL, *AUTO: A program for the automatic bifurcation analysis of autonomous systems*, Congr. Numer., 30 (1981), pp. 265–284.
- [29] I. S. GRADSHTEYN AND I. M. RYZHIK, *Table of Integrals, Series and Products*, 6th ed., Academic Press, San Diego, CA, 2000.
- [30] J. A. SHERRATT, *Numerical continuation methods for studying periodic travelling wave (wave-train) solutions of partial differential equations*, Appl. Math. Comput., 218 (2012), pp. 4684–4694.
- [31] J. A. SHERRATT, supplementary online material, <http://www.ma.hw.ac.uk/~jas/supplements/kl4/>.
- [32] J. D. M. RADEMACHER, B. SANDSTEDTE, AND A. SCHEEL, *Computing absolute and essential spectra using continuation*, Phys. D, 229 (2007), pp. 166–183.
- [33] B. SANDSTEDTE, *Stability of travelling waves*, in Handbook of Dynamical Systems II, B. Fiedler, ed., North-Holland, Amsterdam, 2002, pp. 983–1055.
- [34] F. W. J. OLVER, D. W. LOZIER, R. F. BOISVERT, AND C. W. CLARK, EDS., *NIST Handbook of Mathematical Functions*, Cambridge University Press, New York, 2010.
- [35] P. L. WALKER, *Elliptic Functions: A Constructive Approach*, Wiley, Hoboken, NJ, 1996.
- [36] R. S. MAIER, *Lamé polynomials, hyperelliptic reductions and Lamé band structure*, Phil. Trans. R. Soc. Lond. Ser. A Math. Phys. Eng. Sci., 366 (2008), pp. 1115–1153.
- [37] J. C. EILBECK AND V. Z. ENOL'SKII, *Elliptic Baker-Akhiezer functions and an application to an integrable dynamical system*, J. Math. Phys., 35 (1994), pp. 1192–1201.
- [38] J. A. SHERRATT, *Numerical continuation of boundaries in parameter space between stable and unstable periodic travelling wave (wavetrain) solutions of partial differential equations*, Adv. Comput. Math., to appear.
- [39] M. C. CROSS AND P. C. HOHENBERG, *Pattern formation outside of equilibrium*, Rev. Modern Phys., 65 (1993), pp. 851–1112.
- [40] R. HOYLE, *Pattern Formation: An Introduction to Methods*, Cambridge University Press, Cambridge, UK, 2006.
- [41] G. A. WORRALL, *The Butana grass patterns*, J. Soil Sci., 10 (1959), pp. 34–53.
- [42] J. C. LEPRUN, *The influences of ecological factors on tiger bush and dotted bush patterns along a gradient from Mali to northern Burkina Faso*, Catena, 37 (1999), pp. 25–44.
- [43] X. B. WU, T. L. THUROW, AND S. G. WHISENANT, *Fragmentation and changes in hydrologic function of tiger bush landscapes, south-west Niger*, J. Ecol., 88 (2000), pp. 790–800.

- [44] A. CHAPPELL, C. VALENTIN, A. WARREN, P. NOON, M. CHARLTON, AND J. M. D'HERBES, *Testing the validity of upslope migration in banded vegetation from south-west Niger*, *Catena*, 37 (1999), pp. 217–229.
- [45] K. GUILLAUME, L. ABBADIE, A. MARIOTTI, AND H. NACRO, *Soil organic matter dynamics in tiger bush (Niamey, Niger). Preliminary results*, *Acta Oecologia*, 20 (1999), pp. 185–195.
- [46] D. L. DUNKERLEY, *Infiltration rates and soil moisture in a groved mulga community near Alice Springs, arid central Australia: Evidence for complex internal rainwater redistribution in a runoff-runon landscape*, *J. Arid Environ.*, 51 (2002), pp. 199–219.
- [47] P. M. SACO, G. R. WILLGOOSE, AND G. R. HANCOCK, *Eco-geomorphology of banded vegetation patterns in arid and semi-arid regions*, *Hydrol. Earth Syst. Sci.*, 11 (2007), pp. 1717–1730.
- [48] S. THOMPSON AND G. KATUL, *Secondary seed dispersal and its role in landscape organization*, *Geophys. Res. Lett.*, 36 (2009), L02402.
- [49] J. P. KEENER, *Waves in excitable media*, *SIAM J. Appl. Math.*, 39 (1980), pp. 528–548.
- [50] N. KOPELL AND L. N. HOWARD, *Plane wave solutions to reaction-diffusion equations*, *Stud. Appl. Math.*, 52 (1973), pp. 291–328.
- [51] I. S. ARANSON AND L. KRAMER, *The world of the complex Ginzburg-Landau equation*, *Rev. Modern Phys.*, 74 (2002), pp. 99–143.
- [52] B. SANDSTEDTE AND A. SCHEEL, *Absolute and convective instabilities of waves on unbounded and large bounded domains*, *Phys. D*, 145 (2000), pp. 233–277.
- [53] J. A. SHERRATT, *Invasive wave fronts and their oscillatory wakes are linked by a modulated travelling phase resetting wave*, *Phys. D*, 117 (1998), pp. 145–166.
- [54] S. V. PETROVSKII AND H. MALCHOW, *Wave of chaos: New mechanism of pattern formation in spatio-temporal population dynamics*, *Theor. Popul. Biol.*, 59 (2001), pp. 157–174.
- [55] J. A. SHERRATT, M. J. SMITH, AND J. D. M. RADEMACHER, *Locating the transition from periodic oscillations to spatiotemporal chaos in the wake of invasion*, *Proc. Natl. Acad. Sci. USA*, 106 (2009), pp. 10890–10895.
- [56] M. J. SMITH, J. D. M. RADEMACHER, AND J. A. SHERRATT, *Absolute stability of wavetrains can explain spatiotemporal dynamics in reaction-diffusion systems of lambda-omega type*, *SIAM J. Appl. Dyn. Syst.*, 8 (2009), pp. 1136–1159.
- [57] YU. V. BREZHNEV, *Non-canonical extension of  $\theta$ -functions and modular integrability of  $\vartheta$ -constants*, *Proc. R. Soc. Ed. A*, to appear.
- [58] Y. A. KUZNETSOV, *Elements of Applied Bifurcation Theory*, Springer-Verlag, New York, 2004.
- [59] Y. A. KUZNETSOV, *Andronov-Hopf bifurcation*, *Scholarpedia*, 1(10): 1858, revision 90964, 2006; available online at [http://www.scholarpedia.org/article/Andronov-Hopf\\_bifurcation](http://www.scholarpedia.org/article/Andronov-Hopf_bifurcation).